A DRIVE LASER FOR MULTI-BUNCH PHOTOINJECTOR OPERATION*

D. J. Gibson†, E. Cormier, M. J. Messerly, M. A. Prantil, C. P. J. Barty,
Lawrence Livermore National Laboratory, Livermore, CA, USA

Abstract

Numerous electron beam applications would benefit from increased average current without sacrificing beam brightness. Work is underway at LLNL to investigate the performance of X-band photoinjectors that would generate electron bunches at a rate matching the RF drive frequency, i.e. one bunch per RF cycle. A critical part of this effort involves development of photo-cathode drive laser technology. Here we present a new laser architecture that can generate pulse trains at repetition rates up to several GHz. This compact, fiber-based system is driven directly by the accelerator RF and so is inherently synchronized with the accelerating fields, and scales readily over a wide range of drive frequencies (L-band through X-band). The system will be required to produce 0.5 μJ, $\sim$200 fs rise time, spatially and temporally shaped UV pulses designed to optimize the electron beam brightness. Presented is the current status of this system, producing 2 ps pulses from a continuous-wave source.

INTRODUCTION

Current and future generations of advanced light sources largely depend on high brightness electron beams. LLNL has spent the past decade developing Mono-Energetic Gamma-ray (MEGa-ray) sources by scattering laser light off an electron beam for nuclear physics applications [1, 2]. At the SLAC National Accelerator Laboratory, the Linac Coherent Light Source (LCLS) is generating extraordinarily high peak brightness x-ray beams useful for biological, chemical, and physics studies using a 13.6 GeV Free-Electron Laser (FEL) [3], and Los Alamos is in the process developing the MaRIE (Matter-Radiation Interactions in Extremes) concept, which will also rely on FEL technology [4]. All these light sources would benefit from improved average brightness by increasing the repetition rate of the electron beam source. Since the undulators are based on permanent magnets, they will generate x-rays from as many electron bunches as can be delivered. Similarly, in MEGa-ray sources very little laser light is scattered from each individual electron bunch; if there are additional electron bunches to interact with the laser, they will also scatter photons, generating more gamma-rays.

We are currently setting up an X-band test station capable of delivering 250 pC electron bunches at repetition rates of tens of Hertz with low emittance [5]. Converting this test station to provide a 60 Hz train of macropulses with up to 1000 25 pC micropulses with 11.424 GHz spacing requires optimization of the photoinjector design to handle the new current and space-charge regime [6] as well as a revised laser architecture to generate the electron bunches, presented here.

Table 1: GHz Drive Laser Requirements

Parameter	Cu Cathode	Mg Cathode
Quantum Efficiency	1.0×10^{-5}	1.0×10^{-4}
Micropulses/macropulse	1000	1000
Micropulse Specifications		
Repetition Rate	11.424 GHz	
Pulse Width	250 fs	
Energy @ 260 nm	5 μJ	0.5 μJ
Energy @ 1040 nm	50 μJ	5 μJ
Energy variation	3%	
Macropulse Specifications		
Repetition Rate	120 Hz	
Pulsetrain Length	87.5 ns	
Energy @ 260 nm	5 mJ	0.5 mJ
Energy @ 1040 nm	50 mJ	5 mJ
Energy variation	1%	

DRIVE LASER ARCHITECTURE

The requirements on the drive laser are presented in Table 1 for two options for the cathode material, which impacts the required laser pulse energy. One of the more challenging requirements is locking the laser pulse train precisely to the RF phase, which is required to keep the emittance of all the electron microbunches small. To meet this requirement, we will generate the laser pulse train by modulating a continuous-wave (cw) laser source with a sample of the same RF that drives the accelerator. Several groups [7] have converted cw lasers to sub-ps, high-frequency pulse trains, however these groups have relied on "time-lens" techniques [8] to generate ps-level bandwidths, then used soliton compression at 1550 nm in specially optimized fibers to generate further bandwidth while simultaneously compressing the beam. At the 1 μm wavelengths where we wish to work, the soliton compression scheme isn't feasible because the dispersion in standard fibers has the opposite sign from dispersion at 1550 nm. In the demonstration of this cw-modulation concept reported here, we rely on self-phase modulation (SPM) [9] to generate 1.3 nm of bandwidth and compress the pulse using a standard grating-pair compressor.

* This work performed under the auspices of the U.S. Department of Energy by Lawrence Livermore National Laboratory under Contract DE-AC52-07NA27344

† gibson23@llnl.gov

ISBN 978-3-95450-115-1

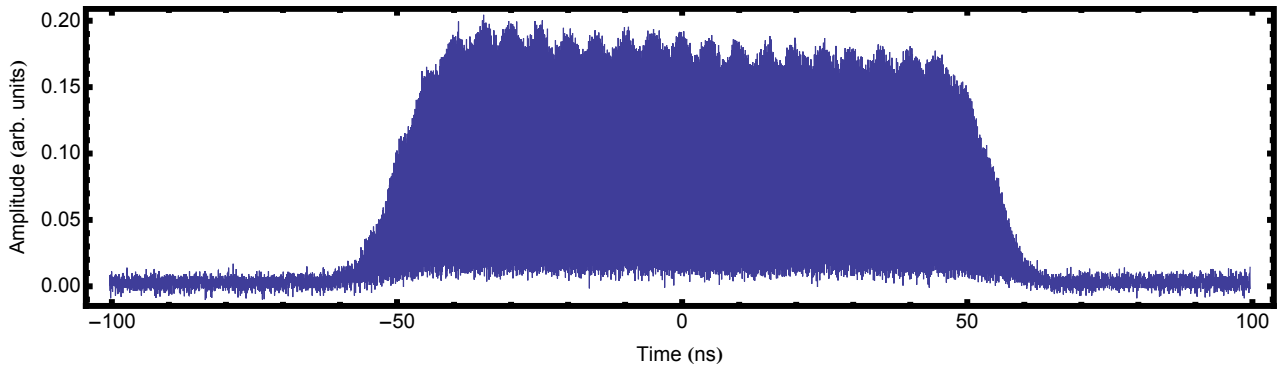

Figure 1: Temporal trace of the laser macropulse recorded using a 12 GHz photodiode. The slow rise and fall times are due to limitations in the pulse-slicing AOM, which will be replaced with a high-speed modulator. The ripple is likely due to a faulty AOM.

The experimental architecture begins with a New Focus Velocity tunable laser set to provide a 1040 nm output. This cw source is sent through an EOSPACE-brand, Z-cut, 20 GHz, dual drive mach-zender electrooptic modulator (EOM) coupled with a feedback circuit which keeps the modulator biased to blick light output. This modulator is driven with 17.3 dBm of 5 GHz RF power. Because of the null bias, the RF drives a 10 GHz laser pulse train at the output of the modulator with ∼50 ps pulse length. The resulting pulse train is amplified by four 6-micron-core, Yb-doped fiber pre-amplifiers. Between each of the preamplifiers is a Crystal Technology acousto optic modulator (AOM). The first of these AOMs slices the 10 GHz modulator ouptut into a 1 MHz train of 100 ns macropulses, each containing approximately 1000 micropulses, as shown in Fig. 1. The slow rise and fall time are a result of physical limitations in the bulk AOMs, and can be eliminated by replacing the first AOM with a high-speed EOM. The 200 MHz amplitude ripple is also an artifact of the AOMs that we expect will be removed when we switch to EOMs. The remaining two AOMs further divide the 1 MHz train down to 200 kHz and 25 kHz, respectively, while simultaneously removing any inter-pulse amplified spontaneous emission.

The output of the preamplifier chain is a 25 kHz, 7 mW pulse train that is then launched into a large-mode area photonic crystal fiber amplifier (Crystal Fibre PZ-40 with a 29 μm mode field diameter), which boosts the power to 150 mW. The pulse train then passes through an optical isolator and is launched into 300 m of 6 μm polarization maintaining fiber where SPM induces bandwidth generation on the signal. Only 42 mW of light is coupled into the SPM fiber. The output can then be measured with an optical spectrum analyzer, a high-speed digital scope using a 12 GHz photodiode, or a custom-built autocorrelator.

PICOSECOND DEMONSTRATION

Figure 2 (top) shows a few possible input pulse shapes that can be generated by driving a null-biased modulator with differing levels of RF voltage relative to the half-wave voltage (V_π) of the modulator. The power has been normalized to yield 6 nJ of energy in each of the pulses. The spectrum expected at the output of the fiber from these shapes can be modeled using the nonlinear Schrödinger equation (NLSE),

$$i\frac{\partial u}{\partial z} - \frac{\beta''}{2}\frac{\partial^2 u}{\partial t^2} + \gamma |u|^2 u = 0, \qquad (1)$$

where u is the complex field envelope, β'' is the second order dispersion term, γ is the nonlinear coefficient, and z is the pulse position along the fiber. Higher order dispersion terms can be included as well, but for the picosecond work presented here, second order is sufficient. The split-step Fourier method is used to numerically solve this equation for the shown pulse shapes propagating through 200 m of 6

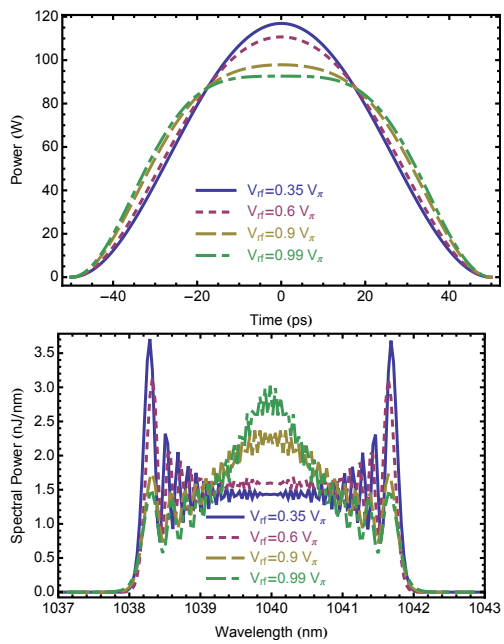

Figure 2: (Top) Temporal profiles launched into 200 m of fiber in a simulation, and (bottom) the resultant spectra. The pulse energy is 6 nJ.

ISBN 978-3-95450-115-1

μm core diameter fiber, and the resultant spectra are shown in the bottom graph of Fig. 2. A strong dependence on pulse shape is seen.

The measured spectrum for our experimental setup at the end of the 300 m of fiber is shown in Fig. 3. For a 42 mW average power beam with a 25 kHz repetition rate, the energy per macropulse is 1.68 μJ, which corresponds to a micropulse energy of $\sim$1.7 nJ. The result of a simulation of this configuration using the NLSE is also plotted in Fig. 3. The pulse shape corresponding to an RF drive voltage of 0.9 V_π is used as an input, and shows excellent agreement on the overall width. The high-frequency oscillations on the measured spectrum correspond to the 10 GHz repetition rate of the measured pulse train.

This pulse train is then passed through a grating pair compressor using multi-layer dielectric gratings with a groove density of 1740 lines/mm. The angle of incidence is 61.8° and the grating slant distance is 290 mm, which was optimized to give the narrowest autocorrelation. Figure 4 shows the measured autocorrelation after the compressor, which has a full-width, half-maximum (FWHM) of 2.7 ps. This corresponds to a pulse width of just under 2 ps. Also shown are the plots of the expected autocorrelation based on the modeling mentioned above (FWHM 2.5 ps) and the autocorrelation expected from a tranform limited pulse with the measured spectrum (FWHM 2.1 ps). All three plots are normalized to the same peak value to allow easy comparison of the widths. The measured spectrum shows a significant amount of power in the wings. This is likely due to the amplitude ripple visible in the macropulse train in Fig. 1. Pulses of different energies will pick up different spectral phases during the SPM process, and so will require different compressor spacings to be fully compressed. Because the autocorrelation shown is actually a simultaneous autocorrelation of all 1000 bunches in the train (we don't slice out a single pulse), the variations in pulse widths result in a broader average autocorrelation.

CONCLUSIONS

We have demonstrated the generation of 1.3 nm of compressible bandwidth and produced a pulse train of 1.7 nJ pulses with 10 GHz spacing in bursts of 1000 pulses each. Having demonstrated the viability of using linac RF to generate a synchronized laser pulse train as well as the ability of SPM to generate bandwidth, we can now add further amplification stages to the system to increase the pulse energy as well as enable further bandwidth generation. Once complete, this system will allow us to generated an 11.424 GHz train of low-emittance electron pulses in our X-band RF gun, significantly increasing the beam current available for Compton-scattering experiments.

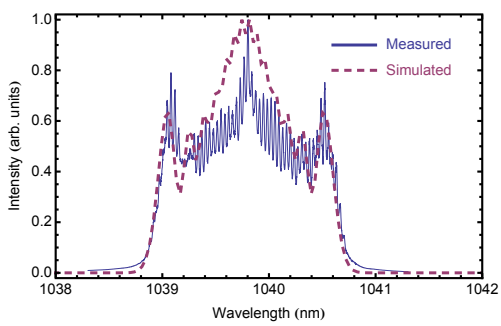

Figure 3: Measured and simulated spectra for a 1.7 nJ pulse traveling through 300 m of fiber.

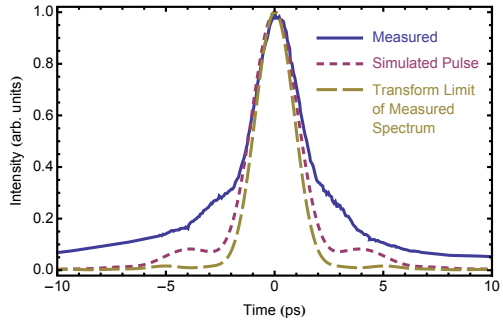

Figure 4: Measured autocorrelation of compressed 10 GHz pulse train after 300 m of fiber. Also shown are the autocorrelations expected from a simulated pulse and from the transform limit of the measured spectrum.

REFERENCES

[1] C. P. J. Barty and F. V. Hartemann, "T-REX: Thomson-Radiated Extreme X-Rays, Moving X-Ray Science into the 'Nuclear' Applications Space...," UCRL-TR-206825, Lawrence Livermore National Laboratory (September 27, 2004).

[2] D. J. Gibson, F. Albert, S. G. Anderson, *et al.*, *Phys. Rev. Spec. Top., Accel. and Beams* **13**, 070703 (2010).

[3] P. Emma, R. Akre, J. Arthur, *et al.*, *Nature Photonics* **4**, 641–647 (2010).

[4] B. E. Carlsten, C. W. Barnes, K. A. Bishofberger , *et al.*, "MaRIE X-Ray Free Electron Laser Pre-Conceptual Design," PAC'11, New York, March 2011, TUODS1, (2011), `http://www.JACoW.org`

[5] R.A. Marsh, *et al.*, "X-band Test Station at LLNL," IPAC'11, San Sebastián, Spain, May 2011, MOPC067, (2011), `http://www.JACoW.org`.

[6] R.A. Marsh, *et al.*, "Modeling Multibunch X-Band Photoinjector Challenges," MOPPP042, these proceedings.

[7] C.-B. Huang, *et al.*, *Elect. Lett.* **42**, 1114 (2006); J. van Howe, *et al.*, *Optics Letters* **32**,1408–1410 (2007); I. Morohashi, *et al.*, *Optics Letters* **34**, 2297–2299 (2009).

[8] T. Kobayashi, H. Yao, K. Amano, *et al.*, *J. Quant. Elect.* **24**, 382–387 (2009).

[9] C. V. Shank, R. L. Fork, R. Yen, *et al.*, *Appl. Phys. Lett.* **40**, 761–763 (1982).

ISBN 978-3-95450-115-1